

RSC Advances



This is an *Accepted Manuscript*, which has been through the Royal Society of Chemistry peer review process and has been accepted for publication.

Accepted Manuscripts are published online shortly after acceptance, before technical editing, formatting and proof reading. Using this free service, authors can make their results available to the community, in citable form, before we publish the edited article. This *Accepted Manuscript* will be replaced by the edited, formatted and paginated article as soon as this is available.

You can find more information about *Accepted Manuscripts* in the [Information for Authors](#).

Please note that technical editing may introduce minor changes to the text and/or graphics, which may alter content. The journal's standard [Terms & Conditions](#) and the [Ethical guidelines](#) still apply. In no event shall the Royal Society of Chemistry be held responsible for any errors or omissions in this *Accepted Manuscript* or any consequences arising from the use of any information it contains.

Amphiphobic surfaces from functionalized TiO₂ nanotube arrays

Samira Farsinezhad¹, Prashant R. Waghmare², Benjamin D. Wiltshire,¹ Himani Sharma,¹ Saeid Amiri,³ Sushanta K. Mitra² and Karthik Shankar^{1,4}

¹Department of Electrical & Computer Engineering, University of Alberta, Edmonton, Alberta T6G 2V4, Canada

²Department of Mechanical Engineering, University of Alberta, Edmonton, Alberta T6G 2V4, Canada

³Wave Control Systems Ltd., 9612-60th Ave. NW, Edmonton AB T6E 0C1

⁴National Institute for Nanotechnology, National Research Council Canada, Edmonton, Alberta T6G 2M9, Canada

*E-mail address of corresponding authors: sushanta.mitra@ualberta.ca, kshankar@ualberta.ca

Keywords: electrochemical anodization, one-dimensional semiconductors, metal oxide nanostructures, Cassie Baxter state, Wenzel state, self-assembled monolayer.

Abstract

Vertically-oriented, self-organized TiO₂ nanotube arrays (TNAs) are a highly ordered *n*-type semiconducting nanoarchitecture with a wide range of potential applications. We generated low energy surfaces repellent to a broad spectrum of liquids by functionalizing TNAs using monolayers of two different fluorinated hydrocarbon molecules: perfluorononanoic acid (PFNA) and 1H, 1H', 2H, 2H'-perfluorodecyl phosphonic acid (PFDPA). Nanotubes of two different outer diameters (50 nm and 130 nm) were studied and their wetting behavior analyzed in liquids belonging to different solvent classes to infer the nature of the wetting states. We show that the wetting behavior of perfluorinated monolayer-functionalized TNAs in polar liquids is explained by *fakir* or Cassie-states whilst the wetting behavior of bare

nanotubes in every liquid is explained by Wenzel-type states. On the other hand, a transition between the Cassie and Wenzel states due to closed pores in the TNA architecture dictates the wetting behavior of functionalized TNAs in apolar liquids. The wetting behavior of functionalized TNAs is understood considering the synergistic effect of geometric and chemical surface modification. PFDPA-functionalized TNAs were found to be resilient to 24 hours of exposure to water and ethylene glycol at a static fluid pressure of 0.105 MPa, and are one step closer towards the realization of a mechanically robust omniphobic surface. At the same time, an understanding of wetting behavior will be useful in the design and optimization of a wide range of interface-sensitive devices such as metal oxide nanotube/nanopore array based sensors, implants, flow-through membranes, photocatalysts and heterojunction solar cells.

Introduction

TiO₂ nanotube arrays (TNAs) are an intriguing class of nanomaterials. They combine the versatile application spectrum of TiO₂ with an ordered porous architecture that is easily achieved by the inexpensive process of electrochemical anodization.¹ The ability of TiO₂ to tether a wide range of biomolecules either directly or through linker monolayers in a stable fashion for extended durations, coupled with the large interfacial area and high effective refractive index of the nanotubes makes TNAs attractive for use in ultrasensitive labeled and label-free optical biosensors.²⁻⁴ TNA-based drug-eluting bone implants utilize the non-toxic, chemically inert and mechanically robust nature of TiO₂, combined with high aspect ratio pores and the resulting diffusion-controlled release of molecules confined in the volume of the pores.⁵⁻¹⁰ The *n*-type semiconducting behavior of TNAs concomitant with the position of the TiO₂ conduction band edge favoring ultrafast (fs) injection from a broad class of dyes, polymers and quantum dots is interesting from the perspective of constructing ordered

excitonic solar cells to overcome both the exciton diffusion bottleneck and to orthogonalize the competing processes of light absorption and charge separation.¹¹⁻¹⁷

A key unifying theme in the above applications is that they all constitute hybrid devices, wherein interfaces involving the TiO₂ nanotubes are critical. These include the dye-TNA, electrolyte-TNA and polymer-TNA interfaces in excitonic solar cells, osteoblast-TNA interface in bone implants, as well as the TNA-biomolecule, TNA-analyte and TNA-foulant interfaces in biosensors. Wetting of the TNA surface by liquids or gels is critical to the functioning of every one of the above-mentioned devices; however, such wetting behavior is currently inadequately understood and poorly optimized for peak device performance. For instance, the resilience of biomolecule-functionalized TiO₂ nanotubes to fouling agents is controlled by the wetting characteristics of the surface. Likewise, the efficiency of the process of filling of *p*-type conjugated polymer(s) into TiO₂ nanotube arrays depends on the wetting properties of the pore-walls with respect to the polymer solution, which in turn dictates the imbibition dynamics of the polymer solution into the pores. In addition, mechanically robust, chemically inert, superamphiphobic coatings have applications in marine and industrial coatings, where the superamphiphobic coatings can retard both the nucleation of inorganic salt crystals and fouling by organic molecules. Despite such remarkable significance, issues concerning wetting rarely figure in the design of devices based on TiO₂ nanotube arrays, and consequently the existing device designs fail to take advantage of the full range of specifications, configurations and performance possibilities associated with the TNA architecture. Systematic and well-designed studies of the wetting behavior of functionalized, well-ordered TNAs are clearly needed to fill this void.

While nanoporous alumina has received some attention as an ordered porous structure for studies of wetting,^{18, 19} self-organized TiO₂ nanotube arrays with inner and outer wall

surfaces and inter-tubular spaces present a different geometry, and potentially different wetting configurations from the hexagonal cylindrical channel architecture of nanoporous alumina. In this paper, we are motivated to generate and understand superamphiphobic surfaces using TiO₂ nanotube arrays. For this purpose, we functionalized titania nanotubes with perfluorinated monolayers since it is well-known that perfluorinated monolayers present the lowest energy surfaces obtainable by purely chemical surface modification.^{20,21} The low polarizability of the C-F bonds and the low overall dipole moment of perfluorinated molecules drastically reduce both Coulombic and Van der Waals interactions²² – this is especially relevant given the high surface energy of the bare TiO₂ surfaces. The combination of chemical and geometric surface modification may be used to generate low energy liquid repellent surfaces with the added advantage of transparency,²³ which are in great demand in diverse applications such as drag-free fluid flow in membranes, spatial confinement of the initiation of chemical reactions, prevention of biofouling, amelioration of fogging and freezing on mirrors and windows, etc. There exist both obvious and subtle differences in wetting phenomena on flat and nanotubular TiO₂ surfaces when functionalized using the same monolayer. For strongly lyophobic monolayers, the annular surfaces of the nanotubes reduce the effective contact area available for wetting and nearly eliminate hysteresis since any imbibition of the solvent droplet into the nanotubes encounters further repulsion from molecules adsorbed on the nanotube walls. On the other hand, in ambient conditions, the imbibition of solvent droplets into nanotubes derivatized by strongly lyophilic monolayers is constrained by the buoyant force of air trapped in the nanotubes.¹⁸ In comparison to textured surfaces that use microstructures, texturing-based on nanostructures is expected to reduce pinning and improve agreement with the Wenzel and Cassie-Baxter theories.²⁴⁻²⁶

A true indication of amphiphobic or superamphiphobic behavior²⁷⁻²⁹ is only obtained by demonstrating liquid repellence of the surface in a broad spectrum of solvents where

dispersion-based, dipole-based and hydrogen-bonding-based interactions are involved. The few extant fundamental studies of wetting behavior on TiO₂ nanotubes are either limited to a narrow range of solvents (mostly from the polar, protic solvent family)³⁰⁻³² and/or utilize nanotubes with visible surface debris,^{31, 33} pore clogging or tangled, randomly oriented morphologies.^{30, 34} Superhydrophobic nanotubes have received far more attention than either oleophobic or amphiphobic nanotube surfaces. Different methods have been used to generate the desired lyophobic behavior. Brush-coating anodized Ti with fluoropolymers has been reported to result in contact angles with water of up to 122°.³⁵ Dip-coating anodized Ti with a perfluoroalkylsilane followed by curing resulted in optimized water contact angles of 150°.³⁶ Superior performance was obtained by forming a monolayer of a perfluoroalkyltrichlorosilane on the exposed surfaces of TiO₂ nanotubes by immersion self-assembly, which resulted in contact angles as high as 163° with water and 157° with ethylene glycol.³⁷ Balaur et al. reported water contact angles of 165-167° by coating TiO₂ nanotube arrays with self-assembled monolayers of octadecylphosphonic acid (ODPA).³¹ In the same study, diameter dependence of the superhydrophobic behavior was also studied and it was found that largest diameter (100 nm) nanotubes provided the highest water contact angles and smallest diameter (20 nm) the lowest contact angles in accordance with the area fraction calculation with Cassie-Baxter theory.³¹ In this report, we study the wetting behavior of clean, unclogged, debris-free TNA surfaces (Fig. 1) coated with linear chain perfluorinated monolayers formed by self-assembly. Two different nanotube diameters and planar films were studied to understand geometric effects. In order to form a perfluorinated monolayer, we chose not to use the commonly employed perfluorinated alkyltrichlorosilane as the coupling agent, due to its well-known propensity to form three-dimensional multilayer polymer films (thus diminishing the structural effect of the nanotubes) and possessing only moderate binding strength to TiO₂ surfaces.³⁸ Instead, we used non-polymerizing perfluorinated alkanephosphonic acid and perfluorinated alkanecarboxylic acid, whose headgroups have

high binding strength to TiO₂ surfaces. We examined many different classes of liquids including polar protic, polar aprotic and non-polar solvents to establish amphiphobicity. We also present a theoretical analysis of the wetting behavior, ensuring that the present work becomes the first systematic study on wetting properties of TNAs providing ample design specifications for future research.

TiO₂ nanotubes have a hardness (> 1 GPa),^{39, 40} Young's Modulus (23-44 GPa)^{40, 41} and fracture toughness (1-2.8 MPa.m^{1/2})⁴² that is either comparable to or higher than films made of polytetrafluoroethylene (PTFE) and other polymers,⁴³ which are currently the predominantly used hydrophobic and amphiphobic surfaces. Therefore, amphiphobic coatings and composites based on TiO₂ nanotube arrays offer the potential of more mechanical robustness, particularly for wear-resistant applications.

Experimental Methods

Materials

Linear chain perfluorononanoic acid (PFNA) with the molecular structure CF₃(CF₂)₇COOH was purchased from Sigma Aldrich Corp. 1H, 1H', 2H, 2H'-perfluorodecyl phosphonic acid (PFDPA) with the molecular structure CF₃(CF₂)₉(CH₂)₂PO₃H₂ was supplied by Aculon Inc. Methanol (99.8%), *n*-hexane (95%), N,N-Dimethylformamide (99.9%), dimethyl sulfoxide (99.9%), diiodomethane, toluene (99.5%), acetone (99.5%), ethylene glycol (99.9%) and ammonium fluoride (98.3%) were obtained from Fisher Scientific. Deionized (DI) water used for contact angle measurements was obtained from ELGA system ((PURELAB Ultra, ELGA).

Preparation of TiO₂ nanotubes and planar TiO₂ thin films

Titanium dioxide nanotube arrays were prepared by electrochemical anodization at room temperature using a two-electrode geometry.⁴⁴ Prior to anodization, titanium foil was degreased ultrasonically in acetone, DI water and methanol for 10 minutes each. The Ti foil

was connected with the electrolyte by an O-ring and formed the anode; the cathode consisted of a piece of titanium with a surface area half time that of the Ti foil.

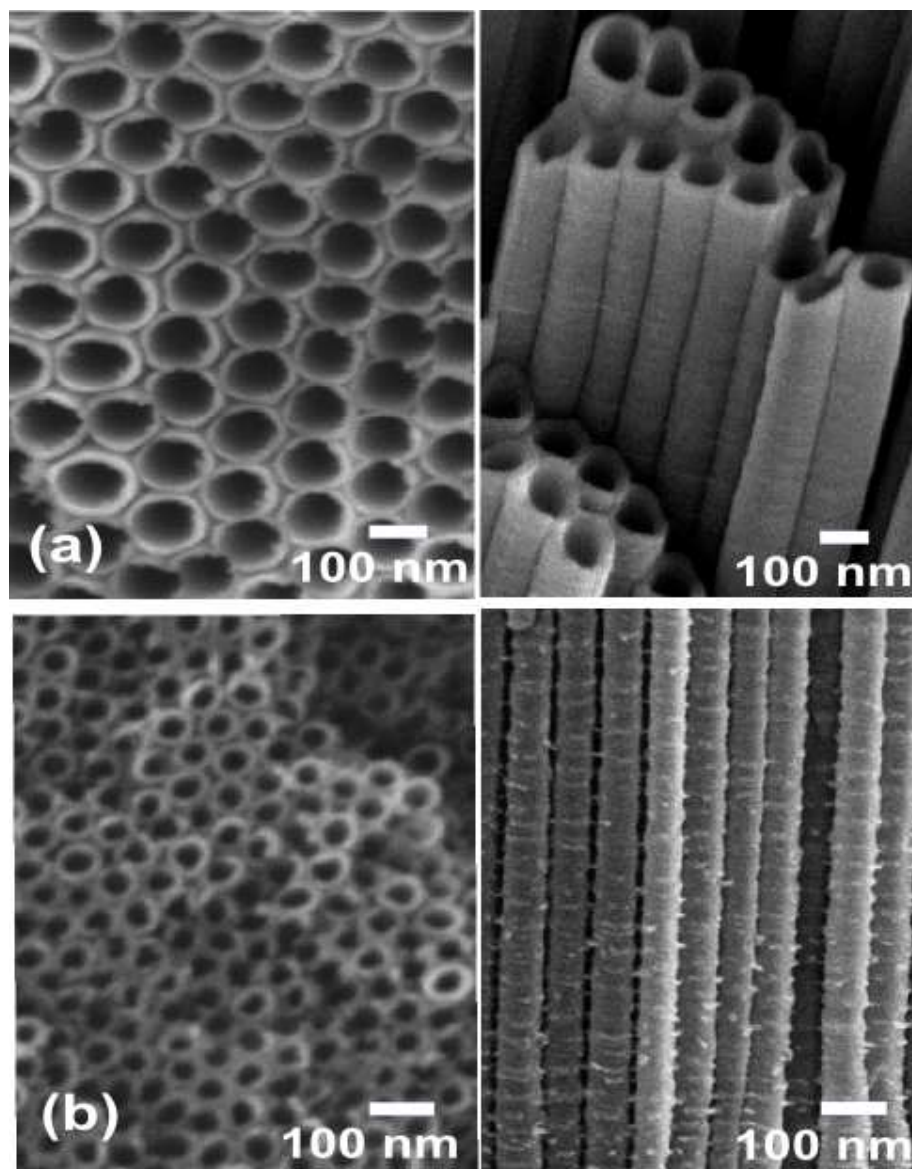


Fig. 1 FESEM images of the two TiO_2 nanotube array geometries used in this study - (a) TNAs of 100 nm average inner diameter formed by anodization at 65 V and (b) TNAs of 30 nm average inner diameter formed by anodization at 20 V.

The distance between the Ti foil and the cathode was approximately 5 cm. A DC power supply was used to drive reaction. For growing highly ordered nanotubes, a two step process involving pre-anodization in the first step, was used. In all steps, the electrolyte

contained 0.3 wt% NH_4F and 4% DI water in ethylene glycol. The pre-anodization step involved anodization of the Ti foil at 65 V for 2 hours followed by ultrasonic delamination of the oxide nanotube layer from the surface to leave a pattern of pits to nucleate ordered nanotubes in the second step. After the first step pre-anodization, the Ti foil was assembled back in the ethylene glycol electrolyte to perform the secondary anodization for another 24 hours. Before the formal anodization, the oxide layer was delaminated ultrasonically, and a pattern was left on the surface of foil. Subsequently, the exposed titanium was used for the first step formal anodization at 65V for three hours followed by rinsing in methanol and drying by pressurized nitrogen. For anodizing small diameter nanotubes, Ti foils were anodized for 72 hours at 20 V and since small diameter nanotubes are more difficult to delaminate, pre-anodization was not used. These TNAs are further treated with oxygen plasma in order to hydroxylate the surface. Concurrently, thin films of planar TiO_2 were prepared by annealing Ti foil overnight on a hot plate at 200° C. The cleaning steps for the Ti foil were identical to those used for the growth of TNAs.

Surface functionalization

Two different molecular monolayers were used to perform the functionalization of planar TiO_2 thin film (TTF), small diameter (TNA_{Small}) and big diameter (TNA_{Large}) titanium dioxide nanotube arrays. Functionalized surfaces were generated by 10 hour immersion in 1 mM solution of perfluorononanoic acid in n-hexane, and in 1 mM perfluorodecane phosphonic acid in methanol, respectively. Functionalization of nanotubes of two different diameters by PFNA and PFDPA resulted in four different kinds of substrates– TNA_{Large}^{PFDPA} , TNA_{Large}^{PFNA} , TNA_{Small}^{PFDPA} and TNA_{Small}^{PFNA} . Systematic wetting studies of TiO_2 thin films (TTF), bare nanotubes (TNA_{Large} and TNA_{Small}) and functionalized thin films, TTF^{PFDPA} and TTF^{PFNA} were performed prior to the measurements of contact angles on TNA_{Large}^{PFDPA} , TNA_{Large}^{PFNA} , TNA_{Small}^{PFDPA} and TNA_{Small}^{PFNA} . Thus, we had in total nine substrates for the contact angle measurements. At least

two samples of each type of substrate were used for contact angle measurements. The complete process flow for the generation functionalized TiO_2 thin films and nanotube arrays is illustrated in Fig. 2.

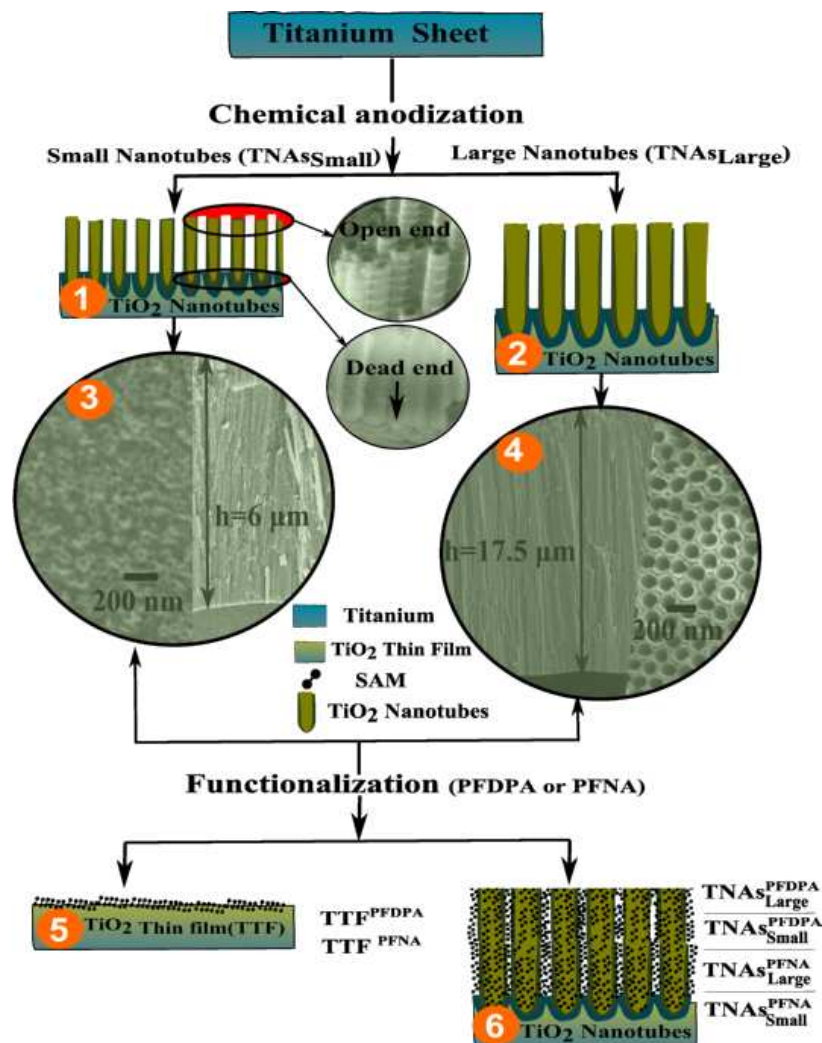


Fig. 2 The process flow for the preparation of the TiO_2 nanotubes coated with perfluoroalkyl monolayers. A Ti foil was used to synthesize the nanotubes by electrochemical anodization. The synthesized TiO_2 nanotubes were of two different types – large and small which are numbered as 1($\text{TNAs}_{\text{Small}}$) and 2($\text{TNAs}_{\text{Large}}$), respectively. The encircled images beside the $\text{TNAs}_{\text{Small}}$ show the SEM images of the top and bottom of the nanotubes. The encircled images at the bottom of $\text{TNAs}_{\text{Large}}$ and $\text{TNAs}_{\text{Small}}$ (image 3 and 4) are the top and side views of the large and small nanotubes. Further, PFNA and PFDA were used to obtain the two different kinds

monolayers by self-assembly on planar TiO₂ thin films (*TTF* –image 5) and *TNA* (image 6) substrates.

Characterization

The morphologies of the TNAs were imaged using a JEOL 6301F Field Emission Scanning Electron Microscope (FESEM). Fig. 1 shows top-views and cross-sections of small diameter and large diameter nanotubes fabricated by the electrochemical anodization process at 65 V and 20 V, respectively. A Thermo Nicolet Nexus670 Fourier Transform Infrared (FTIR) spectrometer was used to obtain vibrational spectra from the sample surfaces in order to verify the presence of the monolayers. X-ray photoelectron spectroscopy (XPS, Kratos Analytical, Axis-Ultra) measurements were conducted using Al K_α source with energy 1486.6 eV under ultra-high vacuum (UHV) conditions ($\sim 10^{-8}$ Torr). The binding energies were calibrated by the C 1s peak of carbon at 284.6 eV. The static contact angle measurements were performed using Drop Shape Analyzer (DSA) 100 (Krüss GmbH - Germany) and the wetting configuration of a 2 μl drop was observed using an in-built CCD camera. The static contact angles were measured on two substrates of each kind (18 substrates in total) and minimum five measurements were performed at different locations on each substrate. In each case, the average contact angle was determined from a series of measurements to evaluate the consistency of wetting behavior on the studied substrate. For measurements of the sustainability of the lyophobic behavior, the wetting configuration of sessile drops was observed before and after 24 hours of immersion in selected solvents using a high resolution digital camera.

Results and Discussion

Verification of functionalization protocols

Fig. 3 shows the XPS spectra of the functionalized TiO₂ thin films and large diameter TNAs. The high resolution spectra of Ti 2p (Fig. 3a) corresponds to two dominant doublet peaks at 10

binding energies of 458.7 eV (Ti 2p_{3/2}) and 464.5 eV (Ti 2p_{1/2}), respectively for TTF^{PFDDPA} and TTF^{PFNA} .⁴⁵ This peak corresponds to the Ti⁴⁺ state of TiO₂. A minor shift of 0.2-0.3 eV is observed for TNA_{Large}^{PFDDPA} and TNA_{Large}^{PFNA} samples. A broadening in the core-level O 1s peak at 530.2 eV (Fig. 3b) for TTF^{PFDDPA} and TTF^{PFNA} samples may be attributed to surface contamination.

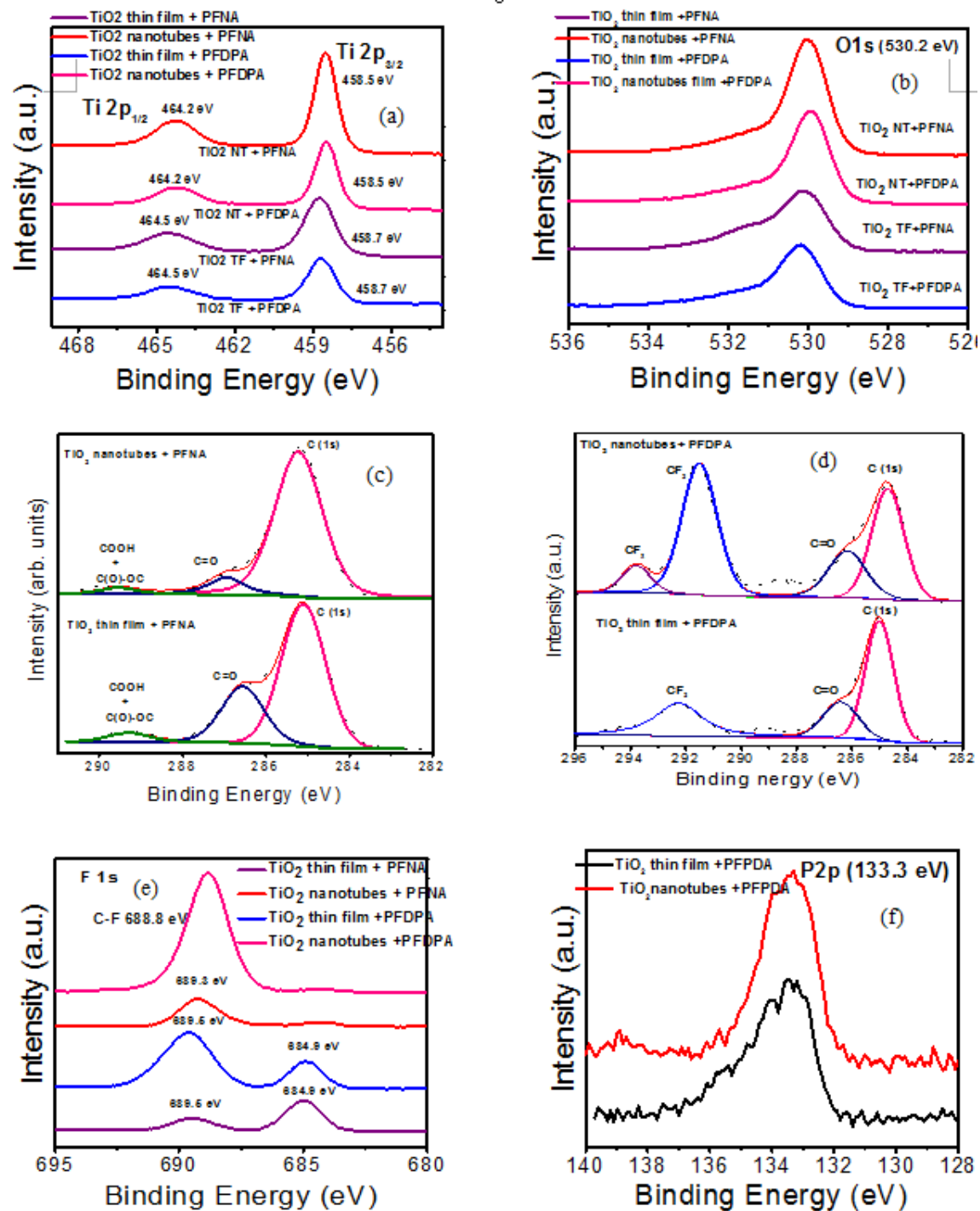


Fig. 3 High resolution XPS spectra of TiO₂ thin films and TNA_{Large} coated with PFNA and PFDPA.

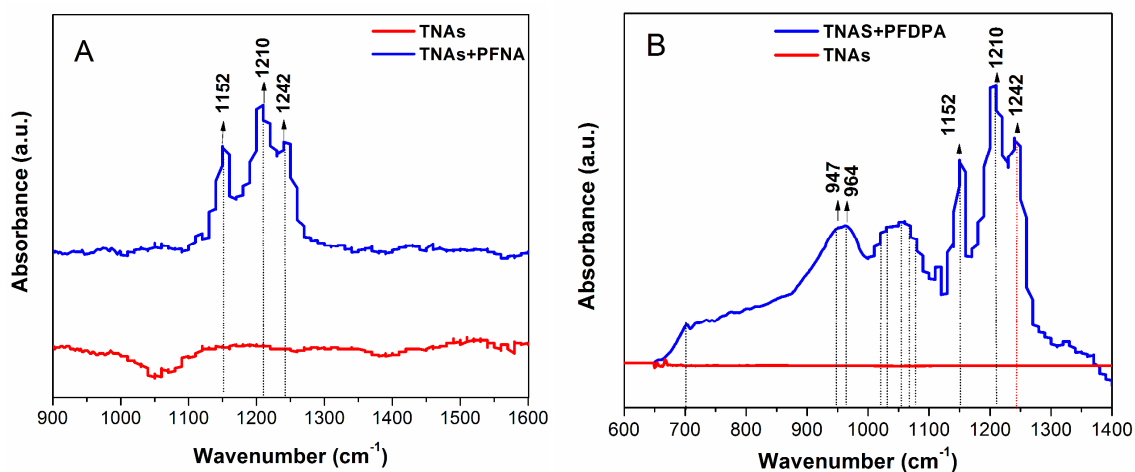


Fig. 4 FTIR spectra of bare TiO₂ nanotube arrays (red), and subsequent to coating (blue) with a monolayer of Perfluorononanoic acid (A) and Perfluorodecylphosphonic acid (B).

The C 1s peaks on TiO₂ surface are deconvoluted into various peaks (Figs. 3c and 3d). The tabulated details of the all the peaks present in the spectra may be found in Table S1 in Supporting Information. The main peak of carbon (C1s) is found at 284.6 ± 0.3 eV in all the samples except that of TTF^{PFNA} .⁴⁶ The C1s peak in the TTF^{PFNA} sample is shifted to 285.1 eV corresponding to C-H bonds on the surface. The other peak found in the C1s region is at 286.4 ± 0.5 eV (C=O), which is found in all the samples. The presence of carboxyl and ester group is seen at binding energies of 288.6 eV and 289.3 eV for the PFNA-coated samples (TTF^{PFNA} and TNA_{Large}^{PFNA}).⁴⁶ No such peak is observed in PFDPA-coated TiO₂ samples (TTF^{PFDPA} and TNA_{Large}^{PFDPA}). However, a prominent peak at binding energy of 291.5 eV is seen in PFDPA-coated TiO₂ samples, corresponding to C-F bonds. This peak is found to be more intense in nanotube samples in comparison to thin films. The presence of C-F bonds is also seen in fluorine (F1s) XPS spectra at binding energy 689 ± 0.5 eV for all the samples (Fig. 3e).

Fig. 3f, shows the P 2p spectra for TTF^{PFDDPA} and TNA_{Large}^{PFDDPA} . The peak with binding energy 133.3 eV corresponds to P 2p_{3/2}, which is attributed to the pentavalent tetra coordinated phosphorous surrounded by different chemical environment.⁴⁷ The 2p line at binding energy of 133.0 eV is found on the surface of an alkane phosphonic acid complexed with zirconium, which was grafted on the native oxide of a Ti plate (TiO₂).⁴⁸ A variation in binding energy of P-2p (132.4 eV to 135.8 eV) is found depending on the oxygen environment. A lowering in binding energy is reported in the P2p when the P-OH bond (at ca. 134.5 eV) in, e.g., CH₃P(O)(OH)₂, is replaced by a P-C bond, as in Ph₂P-(O)OH (133.3 eV). No such peak is found in PFNA based TiO₂ samples.^{49, 50}

Fig. 4 shows the vibrational spectra of the functionalized TNAs. The bands at ca. 1241, 1210 and 1152 cm⁻¹ correspond to the -CF₂ stretches, thus confirming the presence of PFNA and PFDDPA on the surface.⁵¹ In Fig. 4B, the strong -P=O bands in the 1230-1260 cm⁻¹ region are absent while bands in the 1000-1070 cm⁻¹ corresponding to the symmetric ν_sPO₂⁻ are prominent, pointing to a monodentate adsorption of the phosphonic acid headgroup.

Insight into the effect of nanostructuring was obtained by comparing the wetting characteristics of flat TiO₂ films to TNAs for identical functionalization and solvent(s). The packing density of alkanolic acid SAMs is positively correlated to the density of hydroxyl groups on the surface due to the participation of -OH groups in the bidentate binding of -COOH groups to the TiO₂. On the other hand, due to the much stronger interaction of the -PO₃H₂ headgroup with TiO₂, the packing density of alkanephosphonic acid SAMs is independent of the surface -OH group density, and equal to ~1 nmol cm⁻² on a flat TiO₂ substrate, corresponding to an area/molecule of 0.166 nm².⁵²

Effect of surface morphology and surface chemistry on wetting behavior

Our main aim was to fabricate omniphobic substrates which repel a wide range of liquids or solvents. Therefore, we selected polar protic (deionized water, ethylene glycol), polar aprotic (dimethylformamide and dimethyl sulfoxide) and apolar (toluene and diiodomethane) solvents as working liquids for contact angle measurements to characterize the wetting properties of these disparate liquid classes on different chemically modified nanostructures. The measured contact angles for six different liquids on nine different substrates are shown in Fig. 5. The exact values of contact angles with standard deviation in measurement for all six liquids on all nine substrates can be found in the Table S2 in Supplementary Information. The data in Fig. 5, and in Table S2 provide evidence that the chemical treatment, i.e., monolayer formation is necessary for liquid repellence while geometric texturing via the creation of nanotubes generates extreme liquid repellence manifested by large static contact angles $> 140^\circ$.

The influence of the surface chemistry on wetting by particular liquids is commonly analyzed using the Owens-Wendt,⁵³ Fowkes⁵⁴ or Van Oss-Good frameworks⁵⁵ in terms of the dispersive, polar and hydrogen-bonding components of the solid surface energy interacting with the corresponding components of the liquid surface tension. We used the extended Fowkes theory⁵⁶ and the average values of the static contact angle observed using three prototypical liquids with known dispersive, polar and hydrogen-bonding components (diiodomethane, ethylene glycol and water) to determine the components of the solid surface energy, as per the following equations:

$$\gamma_L = \gamma_L^d + \gamma_L^p + \gamma_L^h \quad (1)$$

$$\gamma_S = \gamma_S^d + \gamma_S^p + \gamma_S^h \quad (2)$$

$$\gamma_L(1 + \cos \theta) = 2\sqrt{\gamma_L^d \gamma_S^d} + 2\sqrt{\gamma_L^p \gamma_S^p} + 2\sqrt{\gamma_L^h \gamma_S^h} \quad (3)$$

where γ represents the surface energy, the subscripts S and L denote solid and liquid, respectively while the superscripts d , p and h denote the dispersive, polar and hydrogen-bonding components of the surface energy, respectively. For both liquids and solid surfaces, the total surface energy is given by the sum of the dispersive, polar and hydrogen-bonding components.

While Owens-Wendt, Fowkes and Van Oss-Good theories are strictly applicable only for flat surfaces,⁵⁷ applying them to nanostructured surfaces results in an estimate of the surface energy of a flat substrate that would produce the same static contact angle(s) and allows us predict the overall wetting behavior of nanotube arrays with different types of liquids.⁵⁸ The results of such an analysis are shown in Table S2 in Supporting Information and indicate a strong attenuation of the significant dispersive and hydrogen-bonding surface energies of bare (unfunctionalized) planar and nanotubular TiO₂ surfaces upon perfluoro-functionalization. The extended Fowkes analysis also indicates that nanostructuring the perfluorinated surface produces a near-complete attenuation of polar and hydrogen bonding components of the surface energy. For example, while the polar component of the surface energy (γ_s^p) of the PFNA-functionalized flat TiO₂ sample (*TFF*) drops to 15.56 mN m⁻¹, γ_s^p for PFNA functionalized nanotube samples (TNA_{Small}^{PFNA} and TNA_{Large}^{PFNA}) is < 0.1 mN m⁻¹ (see Table S2). A similar large drop in the hydrogen bonding component of the solid surface energy (γ_s^h) is seen for functionalized nanotube surfaces. Therefore, large static contact angles of wetting are expected for polar protic and polar aprotic solvents on nanotube surfaces, and this is indeed the case for all the polar solvents examined in this study. On the other hand, functionalized nanotube surfaces experienced only a modest decrease (< 3 mN m⁻¹) in the dispersive component (as shown in Table S2) of the surface energy in comparison to perfluorinated flat TiO₂ films. If we closely look at table S2, the total surface energies of the four functionalized nanotube samples (PFNA-large small and PFDPA large and small), are 2.35 mN m⁻¹, 1.03 mN m⁻¹, 0.74 mN m⁻¹ and 1.07 mN m⁻¹, respectively. The maximum

difference in surface energy is 1.61×10^{-3} N/m, which could arise from the assumptions inherent in the extended Fowkes model and is well within the error range of the contact angle measurements. Therefore, while the Fowkes model is useful in understanding the chemical nature of the functionalized surfaces, the predictive value of the surface energy values in estimating the variations in wetting behavior as a function of nanotube morphology, type of functionalization and precise solvent, is quite limited.

Explanation of observed wetting behavior

As mentioned previously, aside from informing us that the functionalized nanotube surfaces have a low overall surface energy with their polar and dispersive components particularly attenuated w.r.t. functionalized flat TiO_2 surfaces, the extended Fowkes analysis of the previous section does not provide sufficient insight into the wetting configuration of different liquids on the various surfaces considered in this study. Therefore, we use a different to approach, outlined here, to analyze the observed wetting behavior. For substrates with geometric non-uniformity and chemical heterogeneity, Wenzel⁵⁹ and Cassie⁶⁰ theories have been widely used to describe the wetting characteristics or contact angles on such substrates. Wenzel suggested that the contact angle of a liquid on a textured surface θ_r^w is a function of surface roughness and the equilibrium contact angle (θ_{flat}^e) on a flat substrate of the same material. This can be expressed as⁵⁹

$$\cos \theta_r^w = r \cdot \cos \theta_{flat}^e \quad (4)$$

where r is the *surface roughness parameter* (ratio of the actual area to the projected area of the substrate containing the nanotextured surface). The theory proposed by Wenzel (Eq.4) indicates that surface roughness always magnifies the inherent wetting property of the substrate i.e. a lyophilic surface becomes even more lyophilic due to surface roughness and a lyophobic surface is rendered even more lyophobic. Therefore, we measured θ_{flat}^e on TiO_2

thin film substrates (*TTF*) and further determined θ_r^w . It was observed that, for all the liquids used in this study, the *TTF* surface is a liquid-attractive surface ($\theta_{flat}^e < 35^\circ$ for all liquids studied). This is attributed to the high surface energy of clean, bare TiO₂ due to dangling bonds and hydroxyl groups on the surface. Nanotubular TiO₂ has an even higher liquid-attractive nature, i.e., the contact angle is smaller than for flat TiO₂ surfaces for all liquids studied.⁶¹ Thus, as predicted by Wenzel⁵⁹ a liquid-attractive bare amphiphilic surface becomes more amphiphilic with the increase in the surface roughness. This observation also implies that the drop placed on the nanotubes is in the Wenzel configuration.

As expected, the formation of a perfluorinated monolayer distinctly changes the wettability of *TTF* substrate. For example, bare *TTF* is hydrophilic, whereas *TTF*^{PFDDPA} and *TTF*^{PFNA} are hydrophobic ($\theta_{flat}^{SAM} > 100^\circ$). However, it is highly challenging to obtain a flat monolayer-coated TiO₂ surface that is truly amphiphobic i.e. shows broad spectrum liquid repellence ($\theta_{flat}^{SAM} > 100^\circ$ for different classes of liquids). To achieve extremely liquid repellent surfaces, we need to obtain a surface where the liquid drop is in Cassie-Baxter or *fakir* state.⁶⁰ The *fakir* state is one that does not allow drop to collapse or spread (on the side walls of nano/micro structure) thereby allowing the liquid to rest at the tip of the asperities on the solid substrate. In such a scenario, the drop is suspended on the micro- or nano-scale asperities with the air underneath it. We performed similar functionalization of the nanotubes as we performed for TiO₂ thin films. It was observed by us that the nanotubes functionalized with perfluorinated monolayers showed extreme liquid repellence (Fig. 5), for example *TTF*^{PFDDPA} is hydrophobic in nature but monolayer-coated TNAs (TNA_{Large}^{PFDDPA} , TNA_{Large}^{PFNA} , TNA_{Small}^{PFDDPA} and TNA_{Small}^{PFNA}) show superhydrophobic behavior ($\theta_{TNAs}^{SAM} > 170^\circ$). The detailed analysis and explanation of such behavior is provided in a later section.

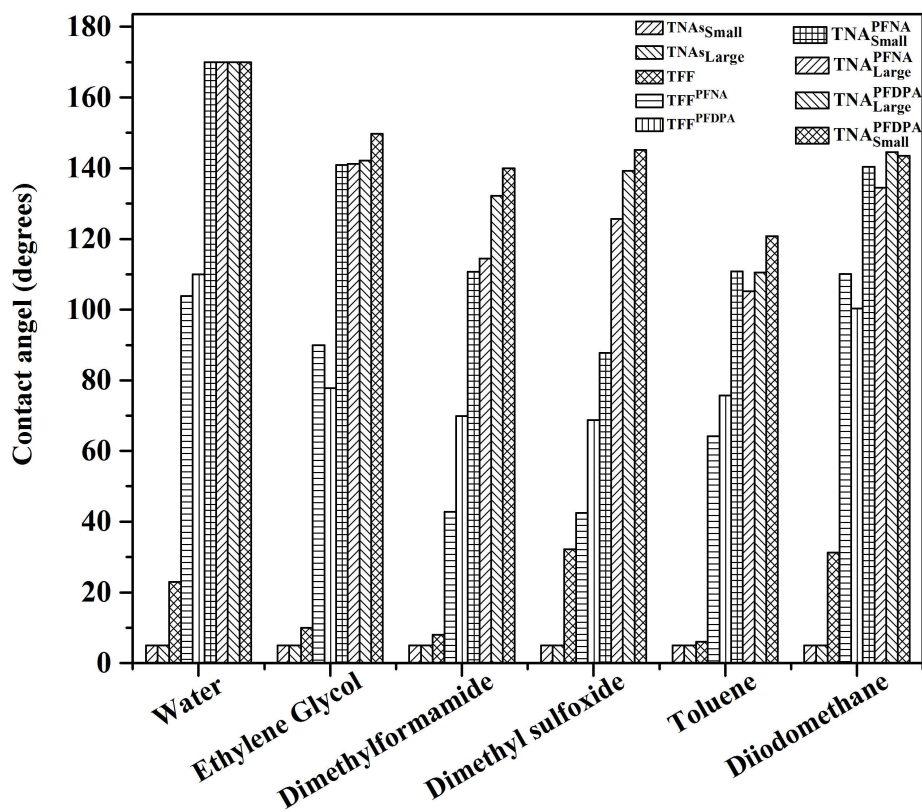


Fig. 5 Equilibrium contact angles of different liquids on nine different substrates measured by the pendant drop technique are presented here. The bare TiO_2 thin film allows all liquids considered in this study, to spread easily; in nanotubular form (TNA_{Large} and TNA_{Small}), the substrates became more amphiphilic. The chemical treatment, namely functionalization by two different perfluorinated alkane chain-containing molecules (PFNA and PFDA) resulted in the bare flat TiO_2 thin films becoming hydrophobic surfaces (TFF^{PFDA} and TFF^{PFNA}). A similar treatment was performed on two different nanotubes (TNA_{Large} and TNA_{Small}) to generate four types of functionalized nanotube array samples (TNA_{Large}^{PFDA} , TNA_{Large}^{PFNA} , TNA_{Small}^{PFDA} and TNA_{Small}^{PFNA}), which showed distinctly different liquid-repellent characteristics compared to the bare nanotubes. The static contact angles obtained with these functionalized nanotubes are some of the highest observed for any surface.

Analysis of wetting properties and theoretical predictions of contact angle

In the case of a structurally heterogeneous surface, such as TNA_{Large}^{PFDDPA} , TNA_{Large}^{PFNA} , TNA_{Small}^{PFDDPA} and TNA_{Small}^{PFNA} , Cassie and Baxter reported that the contact angle of a liquid drop on a heterogeneous substrate in an air medium can be expressed as⁶⁰

$$\cos\theta_r^{CB} = f_{sl} \left(1 + \cos\theta_{flat}^e\right) - 1 \quad (5)$$

where f_{sl} is the *contact area fraction parameter*, i.e., the ratio of the liquid-solid contact area and the projected area of the drop base. Titania nanotubes formed by anodization in ethylene glycol electrolytes are known to pack in a triangular lattice. The unit cell for the observed TiO_2 arrangements (see Fig. 1 and images (a) – (c) in Fig. 6) can therefore be considered as an equilateral triangle, of side $2R_0$ (for nanotubes without any gap) or $2R_0+s$ (for nanotubes with gap s) formed due to three hollow nanotubes. The representative unit cell considered for the analysis and the top view of this unit cell is shown in Fig. 6b. For this case, the contact area fraction parameter (f_{sl}) can be presented as,

$$f_{sl} = \frac{\frac{2t}{R_0} - \left(\frac{t}{R_0}\right)^2}{\frac{2\sqrt{3}}{\pi} \left[1 + \left(\frac{s}{2R_0}\right)^2\right]} \quad (6)$$

where R_0 and t are the outer radius and thickness of an individual nanotube, respectively and s is the inter-tube spacing. For each of the two nanotube architectures studied, the values of R_0 , t and s were extracted using scanning electron micrographs, and are shown in Table S3. Table 1 shows the comparison between the experimentally measured contact angle and the difference between the experimentally measured and theoretically predicted (using Eqs. 5 and 6) contact angles. The subscript and superscript of the contact angle (θ) in Table 1 represent the type of nanotube and the functionalization process, respectively. The value in the parenthesis represents the percentage difference between the theoretical predictions and

experimentally observed contact angle measurements. It is evident that the TNA_{Small}^{PFDDPA} surface is the most liquid repellent surface with minimal deviation from the theoretical prediction.

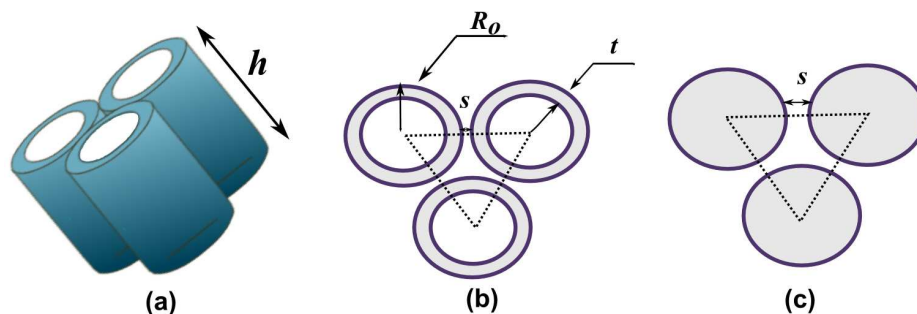


Fig. 6 (a) The unit cell considered for the theoretical analysis assumes that the nanotubes are closely packed in a triangular lattice (b) First scenario considered for the analysis: the unit cell consists of three hollow nanotubes with height h , radius R_0 , wall-thickness t and inter-tube spacing s . (c) Second scenario considered for the analysis: The nanotubes are considered as solid nanorods of outer radius R_0 and there is a finite gap s in between them.

Liquid	θ_{Large}^{PFNA}	$\Delta\theta_{Large}^{PFNA}$	θ_{Large}^{PFDDPA}	$\Delta\theta_{Large}^{PFDDPA}$
Ethylene Glycol (EG)	141.18±5.5	4.46 _(3.16)	142.2±1.32	11.20 _(7.87)
Dimethylformamide (DMF)	114.5±5.9	6.01 _(5.25)	132.2±0.53	3.99 _(3.02)
Dimethyl sulfoxide (DMSO)	125.7±3.5	5.25 _(4.17)	139.3±1.44	11.50 _(8.25)
Toluene	105.2±0.8	21.31 _(20.29)	110.5±0.91	14.74 _(12.75)
Diiodomethane (DIM)	134.5±1.59	9.95 _(7.40)	144.6±0.38	4.93 _(3.39)
Liquid	θ_{Small}^{PFNA}	$\Delta\theta_{Small}^{PFNA}$	θ_{Small}^{PFDDPA}	$\Delta\theta_{Small}^{PFDDPA}$
Ethylene Glycol	140.9±4.5	24.45 _(17.41)	149.7±.22	42.31 _(28.26)
Dimethylformamide	110.7±2.5	20.90 _(19.01)	140.0±4.92	37.15 _(26.53)
Dimethyl sulfoxide	87.8±23.3	1.89 _(2.14)	145.2±2.61	43.02 _(29.62)
Toluene	110.8±3.44	11.09 _(10.12)	120.8±2.17	14.64 _(12.21)
Diiodomethane	140.4±3.39	12.07 _(8.59)	143.5±0.88	21.854 _(15.22)

Table 1. The experimentally measured contact angle (θ) and deviation ($\Delta\theta$) from theoretically predicted value. The value in the parenthesis represents the percentage difference between the theoretically predicted and experimentally measured contact angle values.

Both Table 1 and Table S2 show that PFDPA-coated nanotube surfaces exhibit high contact angles ($> 130^\circ$) approaching superamphiphobic behavior for the four polar solvents examined in this study, namely water, EG, DMF and DMSO. PFNA-coated nanotube surfaces exhibit contact angles $> 140^\circ$ for the protic solvents (water and EG), and lower contact angles for the aprotic solvents, DMF and DMSO (Table S2). On the other hand, perfluoro-functionalized flat TiO_2 surfaces (TFF^{PFNA} and $\text{TFF}^{\text{PFDPA}}$) repel protic solvents and do not repel aprotic solvents (Table S2). Thus for the polar aprotic solvents (DMF and DMSO), the liquid attractive behavior of the TFF^{PFNA} and $\text{TFF}^{\text{PFDPA}}$ transforms to liquid repellent behavior for the functionalized nanotubes, pointing to the likely emergence of Cassie-Baxter type wetting states. For polar protic solvents (Water and EG), the liquid-repellent behavior of TFF^{PFNA} and $\text{TFF}^{\text{PFDPA}}$ is amplified by nanostructuring, which could be caused by either Cassie-Baxter or Wenzel-type wetting states. Our subsequent analysis attempts to determine the nature of this wetting state. Keeping in mind that each nanotube behave as a closed pore and the inter-tube spaces act as an open space, we deduce that a liquid droplet may exist in three different configurations on the perfluorinated monolayer-coated nanotubes as shown in Fig. 7. In each configuration, the local interaction between the individual nanotube and the liquid-air interface dictates the outcome of the drop configuration. In the first configuration, the drop does not spread locally on either the outer or inner surfaces of the nanotubes and consequently, we observe the failure in the drop deposition with the conventional pendant drop deposition technique.²³ The pendant drop deposition technique is a widely adopted technique to deposit the drop on the substrate for contact angle measurements where the needle with a liquid drop at its tip is brought near to the characterizing substrate and further allowed to get deposit on the substrate. During the deposition, the drop detaches from the needle and spreads on the substrate and finally one can determine the equilibrium contact angle of the drop which is in equilibrium condition on the substrate. It is to be noted that to determine the wetting characteristics of any low energy

surface (the surface with very high contact angles) the drop volume needs to be smaller so that the contact angle measurements are performed without any influence of gravity.⁶² This is achieved by maintaining the drop radius (R_c) much smaller than capillary length scale $l_c = \sqrt{\gamma/\rho g}$ where γ , ρ and g are the liquid surface tension, liquid density and the gravitational acceleration respectively. In the case of very low energy surface such as functionalized *TNA* surfaces where the water drop of radius $\leq R_c$ remains attached to the needle and does not spread on the substrate. If we apply additional force on the drop through the needle to obtain the forceful spreading, first the drop rolls/slides on the characterizing surface and then climbs-up on the needle outer surface (Refer to Supplementary Video in Waghmare et al.⁶³). Since in our case the height of the nanotube is much larger than the radius h ($\sim 6-18 \mu\text{m}$) $\gg R_0$ (38-75 nm), the developed stresses at the three phase contact line (the portion at which drop is in contact with solid substrate) may disturb the nanotube arrangement.^{63, 64} Moreover, if we perform the contact angle measurements on the drop that is attached to the needle, it may lead to wrong interpretation of the contact angles because the drop in this configuration always has affinity towards the needle. We have also maintained the drop-substrate contact for a longer time ($> 1 \text{ min}$) to allow the drop to spread without any additional force from the needle on the drop. But it was observed that the drop never spreads on the substrate and remained attached with the needle. Further, if the needle is retracted away from the characterizing substrate the drop travels along with the needle. For ultralyophobic surfaces, sessile drops of larger volume were used to observe the wetting behavior - but contact angles measured in such a configuration include the effect of gravity. For such ultralyophobic cases (e.g. water on functionalized nanotubes in this study) where a drop never gets deposited or spread on the surface, we have reported the contact angle $> 170^\circ$. In such a scenario, the drop neither stays in contact with any portion of the nanotube nor spreads locally as shown in the first configuration (image 1) of Fig. 7.

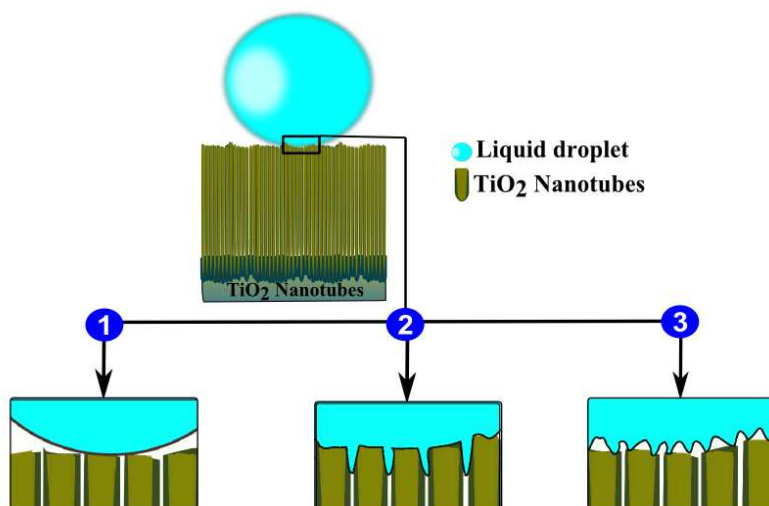


Fig. 7 Possible drop configuration of liquids during the contact angle measurements. In the first case, the drop does not spread, whereas in the second and third cases the drop spreads over areas which are different from the area predicted by the contact area fraction parameter.

For polar liquids other than water, we surmise that the liquid either spreads locally on the nanotube surface (image 2) or is in contact with a certain portion of the nanotube to-surface (image 3) as shown in Fig. 7. Whether the liquid just spreads on the tip of the nanotubes or if it imbibes in between the nanotubes or inside the nanotubes, is ambiguous. However, in our analysis thus far, we have strictly considered the drop is able to access only the top surface of the nanotubes for spreading, and therefore the geometric feature of the tip of the nanotubes (R_0 and t in Eq. 6) decides the outcome of the drop configuration (using Eq. 5). It is necessary to further investigate the local spreading of the drop to find out whether the drop has partially wetted the outer nanotube surface or whether it has imbibed inside the nanotubes. For this purpose, we have defined the experimental area fraction parameter (f_{sl}^{exp}) as follows⁶⁵

$$f_{sl}^{\text{exp}} = \frac{1 + \cos \theta_{TNAs}^e}{1 + \cos \theta_{flat}^e} \quad (7)$$

and compared it with the theoretically determined area fraction parameter (f_{sl}) provided in Eq. (6). In Eq. (7), $\cos \theta_{TNA_s}^e$ is the equilibrium contact angle measured on TNA surfaces. If $f_{sl}^{\text{exp}} > f_{sl}$, then the drop wets the external surface (as shown in image 2 of Fig. 7) in addition to the top surface of the pillar-like micro/nano structure. This results in over-prediction of the equilibrium contact angles. In the alternative case, where $f_{sl}^{\text{exp}} < f_{sl}$, the drop is in contact with less area compared to the minimum available area to spread (as depicted in image 3 of Fig. 6) or the area predicted by theory. The geometrical parameters (f_{sl}^{exp} and f_{sl}) for different nanotube configurations are presented in Table 2. The area fraction parameters for our cases are determined by using geometric parameters of nanotubes (Eq. 6 and Supplementary Table S3) and the experimentally observed contact angle values (Eq. 7 and Supplementary Table S2). The number in the parenthesis after the sample name in Table 2 provides the theoretical area fraction parameter (f_{sl}) for four different configurations. Subsequently, the experimental area fraction parameter (f_{sl}^{exp}) for the same substrates with different liquids is also presented. It is to be noted that the experimental area fraction parameter (f_{sl}^{exp}) is determined from the contact angle values obtained from experiments and hence f_{sl}^{exp} is different for each liquid even though the drop is resting on the same geometric configuration whereas the theoretical area fraction parameter (f_{sl}) is purely a function of the geometrical parameters. It is clear from Table 2 that for the majority of studied substrate and liquid combinations $f_{sl}^{\text{exp}} < f_{sl}$, which suggests that these liquids prefer to be in contact with the air rather than the TiO₂ surface, and we infer that the drop is in a similar configuration to that presented in image 3 of Fig. 7. Thus, we can infer the liquid drop to be in the *fakir* state, where the drop sticks to the surface but does not spread on the available surface. The reduction in contact area over and above that expected from purely geometrical considerations could be local surface roughness on the axial surface of the nanotubes and the type of

molecular packing on the substrate. It is well-known that perfluorinated monolayers occupy an effective area 1.5 times that of the analogous alkane chains and are rigidly oriented almost orthogonally from the surface (i.e. parallel to the surface normal) due to the helical arrangement of CF_2 segments.⁶⁶ Due to the above mentioned larger spacing between adjacent molecules and the weaker Van der Waals interactions involving the less polarizable C-F bonds, the packing density of perfluorinated monolayers is smaller than that of alkyl chains. According to Hamaker theory,^{67, 68} close-packed monolayers experience stronger interactions with chemically similar molecules while a smaller molecular packing density results in weaker interactions, and therefore a larger contact angle than expected from purely chemical similarity between the molecules in the liquid and on the solid surface. These factors could explain why f_{sl}^{exp} is smaller than f_{sl} , and not equal to it. The clear exceptions to the plausible formation of *fakir* states are the wetting of toluene by TNA_{Large}^{PFNA} and TNA_{Large}^{PFDDPA} , and diiodomethane by TNA_{Large}^{PFNA} . In these cases, $f_{sl}^{\text{exp}} > f_{sl}$ implying the liquid is wetting an area larger than dictated by the geometry of the nanotube top-surface.

Sample	TNA_{Large}^{PFNA}	TNA_{Large}^{PFDDPA}	TNA_{Small}^{PFDDPA}	TNA_{Small}^{PFNA}
f_{sl}	(0.2842)	(0.2842)	(0.5803)	(0.5803)
	f_{sl}^{exp}	f_{sl}^{exp}	f_{sl}^{exp}	f_{sl}^{exp}
Ethylene Glycol	0.23	0.18	0.05	0.23
Dimethylformamide	0.34	0.25	0.17	0.37
Dimethyl sulfoxide	0.24	0.18	0.13	0.60
Toluene	0.52	0.52	0.39	0.45
Diiodomethane	0.46	0.28	0.24	0.36

Table 2. The area fraction parameter derived from experiments using Eq. 6. And Eq 7. The corresponding theoretical values, based on Eq. (3), are provided in parenthesis beside each different nanotube arrays.

One may also argue that the base of the nanotube is always encapsulated, since the nanotube grows from the base, whereas the other end is always open (please see encircled

SEM pictures in image 3 of Fig. 2, i.e., open end and dead end). Thus, the entrapped air inside the nanotube pores may not find a way to get displaced if the liquid attempts to imbibe inside the nanotubes. In this situation the liquid may pressurize the entrapped air inside the nanotube instead of displacing it, and eventually the liquid may prefer the wetting of the external wall of nanotubes. The choice of configuration 2 (image 2 in Fig. 7) as a possible alternative to the formation of *fakir* states is influenced by recent studies on closed pore structures^{18, 69} strongly suggesting that trapped air does indeed resist the imbibition of liquid inside the pores. In such cases, one can consider the hollow tube act as a solid cylindrical pillar or as a nanorod, where the liquid can only spread on the outer surface of the nanorods. Owing to this argument, we have also performed the analysis for the case where we have assumed that the hollow nanotubes behave as a nanorod with a finite gap (s) in between them as shown in Fig. 7c. The theoretical contact area fraction parameter (f_{sl}^{rod}) for such arrangement is

$$f_{sl}^{rod} = \frac{\pi}{2\sqrt{3}} \left(1 + \frac{s}{2R_0} \right)^{-2} \quad (8)$$

The supplementary Table S4 shows the difference between the measured contact angles and the theoretically determined contact angles, using Eqs. (8) and (5). It is distinctly clear that the deviation between the theoretical value and the experimentally measured contact angle for this case is much larger than the deviation observed in previous case (Table 1) i.e., the hollow nanotubes, lending further support to our speculation of drop configurations presented in Fig. 7 the formation of *fakir* states during wetting of functionalized nanotubes by polar liquids.

Now we try to understand the wetting configurations in Table 2 that result in $f_{sl}^{exp} > f_{sl}$. In the case of the weakly polar liquids toluene and diiodomethane (DIM), wetting behavior different from that of polar liquids is encountered on the functionalized nanotube surfaces. Table S1 shows that toluene wets flat TiO₂ (*TFF*), functionalized TiO₂ thin films –

TFF^{PFNA} and TFF^{PFDDA} (contact angles $< 90^\circ$) and bare nanotubes (TNA_{Large} and TNA_{Small}) whereas, it poorly wets functionalized TiO_2 nanotubes (contact angles $> 90^\circ$). Such a transformation in wetting behavior is indicative of a Cassie-Baxter state, but the corresponding increase in the static contact angle falls significantly short of the minimum contact angles expected from the Cassie-Baxter relation for TNA_{Large}^{PFNA} and TNA_{Large}^{PFDDA} . Flat, functionalized TFF surfaces repel DIM and this behavior is amplified in functionalized nanotubes, but likewise not to the extent expected from the Cassie-Baxter relation, for TNA_{Large}^{PFNA} . At the same time, the contact angles observed for this case diverge from the values expected for a classic Wenzel-state accounting for the complete surface area of the nanotubes. The results are suggestive of partial imbibition of toluene and DIM into the nanotubes (image 2 in Fig. 6), which corresponds to a transition between the Cassie-Baxter and Wenzel regimes.

In order to characterize the sustainability of the amphiphobic coating, separate samples of large diameter nanotube arrays functionalized by PFNA (TNA_{Large}^{PFNA}) and PFDPA (TNA_{Large}^{PFDPA}) monolayers were immersed under 35 cm of water and ethylene glycol respectively for a full day, thus subjecting the coatings to a static fluid pressure of 0.105 MPa over a period of 24 hours. The static contact angle was measured before and after the immersion treatment. For PFNA monolayers, the surface became hydrophilic after being immersed for only a few minutes, due to the hydrolyzed desorption of the chemisorbed carboxylate linkages on the TiO_2 . On the other hand, for PFDPA monolayers tethered to the TiO_2 nanotubes by the water-stable phosphonate linkages, the contact angle was unchanged due to the immersion treatment (Figs. S3 and S4 in Supporting Information).

Conclusions

It is well understood that the chemical heterogeneity and surface topography significantly influence the wetting characteristics of the substrate. The chemical heterogeneity is either achieved by the chemical treatment¹⁷ or heat treatment,⁷⁰ whereas specific surface topographies are obtained by texturing the surface by fabricating micro/nanostructures.⁷¹ However, obtaining a superomniphobic surface i.e. one that can repel a wide range of liquids (such as polar, non-polar, protic, aprotic, organic, non-organic, etc.), is still an unresolved issue. Here, we have attempted to produce a substrate that repels a wide range of liquids. We have combined both approaches – the geometric texturing (by growing TiO₂ nanotubes on the substrates) and chemical heterogeneity (by functionalizing the TiO₂ surface with liquid-repellent monolayers) to achieve this goal. The necessity of such a combined approach is validated by presenting the wetting characteristics of two different configurations of TiO₂ nanotubes with and without chemical treatment. Secondly, the highly ordered nanotube architecture presents a model system to study wetting and imbibition processes. The functionalization of TiO₂ nanotube arrays with perfluorodecanephosphonic acid generated a surface which can be considered an omniphobic surface since it repelled a wide range of liquids (polar protic, polar aprotic and select non-polar solvents).

Acknowledgements

This work was made possible by direct financial support or indirect (equipment) support from the Natural Sciences and Engineering Research Council of Canada (NSERC), the Canada Foundation for Innovation (CFI), the Alberta Small Equipment Grants Program, CMC Microsystems and the National Research Council of Canada (NRC). SF thanks Alberta Innovates Technology Futures for scholarship support.

References

1. K. Shankar, in *Encyclopedia of Nanotechnology*, ed. B. Bhushan, Springer Netherlands, 2012, ch. 382, pp. 2742-2755.
2. K. S. Mun, S. D. Alvarez, W. Y. Choi and M. J. Sailor, *Acs Nano*, 2010, 4, 2070-2076.
3. Y. Y. Song, F. Schmidt-Stein, S. Berger and P. Schmuki, *Small*, 2010, 6, 1180-1184.
4. P. Kar, A. Pandey, J. J. Greer and K. Shankar, *Lab Chip*, 2012, 12, 821-828.
5. I. De Santo, L. Sanguigno, F. Causa, T. Monetta and P. A. Netti, *Analyst*, 2012, 137, 5076-5081.
6. K. Gulati, S. Ramakrishnan, M. S. Aw, G. J. Atkins, D. M. Findlay and D. Losic, *Acta Biomater.*, 2012, 8, 449-456.
7. M. Kazemzadeh-Narbat, B. F. L. Lai, C. F. Ding, J. N. Kizhakkedathu, R. E. W. Hancock and R. Z. Wang, *Biomaterials*, 2013, 34, 5969-5977.
8. K. Liang, X. C. Li and B. K. Tay, *Nanosci. Nanotechnol. Lett.*, 2013, 5, 162-166.
9. S. Oh, K. S. Moon, J. H. Moon, J. M. Bae and S. H. Jin, *J. Nanomater.*, 2013.
10. K. C. Papat, M. Eltgroth, T. J. La Tempa, C. A. Grimes and T. A. Desai, *Small*, 2007, 3, 1878-1881.
11. L. Luo, C. J. Lin, C. Y. Tsai, H. P. Wu, L. L. Li, C. F. Lo, C. Y. Lin and E. W. G. Diau, *Phys. Chem. Chem. Phys.*, 2010, 12, 1064-1071.
12. W. T. Sun, Y. Yu, H. Y. Pan, X. F. Gao, Q. Chen and L. M. Peng, *J. Am. Chem. Soc.*, 2008, 130, 1124-+.
13. H. H. Yang, W. G. Fan, A. Vaneski, A. S. Susha, W. Y. Teoh and A. L. Rogach, *Adv. Funct. Mater.*, 2012, 22, 2821-2829.
14. M. Ziolk, B. Cohen, X. C. Yang, L. C. Sun, M. Paulose, O. K. Varghese, C. A. Grimes and A. Douhal, *Phys. Chem. Chem. Phys.*, 2012, 14, 2816-2831.
15. K. Shankar, J. Bandara, M. Paulose, H. Wietasch, O. K. Varghese, G. K. Mor, T. J. LaTempa, M. Thelakkat and C. A. Grimes, *Nano Letters*, 2008, 8, 1654-1659.
16. K. Shankar, G. K. Mor, M. Paulose, O. K. Varghese and C. A. Grimes, *Journal of Non-Crystalline Solids*, 2008, 354, 2767-2771.
17. S. Kim, G. K. Mor, M. Paulose, O. K. Varghese, K. Shankar and C. A. Grimes, *Ieee Journal of Selected Topics in Quantum Electronics*, 2010, 16, 1573-1580.
18. Z. Li, J. Wang, Y. Zhang, J. Wang, L. Jiang and Y. Song, *Applied Physics Letters*, 2010, 97, -.
19. S. Smirnov, I. Vlassiuk, P. Takmakov and F. Rios, *ACS Nano*, 2010, 4, 5069-5075.
20. F. Schulman and W. A. Zisman, *Journal of Colloid Science*, 1952, 7, 465-481.
21. E. F. Hare, E. G. Shafrin and W. A. Zisman, *The Journal of Physical Chemistry*, 1954, 58, 236-239.
22. D. F. Cheng, B. Mashed, C. Urata and A. Hozumi, *Langmuir*, 2013, 29, 11322-11329.
23. P. R. Waghmare, S. Das and S. K. Mitra, *Sci Rep*, 2013, 3.
24. J. F. Joanny and P. G. de Gennes, *The Journal of Chemical Physics*, 1984, 81, 552-562.
25. S. Brandon, N. Haimovich, E. Yeger and A. Marmur, *Journal of Colloid and Interface Science*, 2003, 263, 237-243.
26. G. Wolansky and A. Marmur, *Colloids and Surfaces A: Physicochemical and Engineering Aspects*, 1999, 156, 381-388.
27. A. Tuteja, W. Choi, M. L. Ma, J. M. Mabry, S. A. Mazzella, G. C. Rutledge, G. H. McKinley and R. E. Cohen, *Science*, 2007, 318, 1618-1622.
28. J. Zhang and S. Seeger, *Angew. Chem.-Int. Edit.*, 2011, 50, 6652-6656.
29. X. Deng, L. Mammen, H. J. Butt and D. Vollmer, *Science*, 2012, 335, 67-70.

30. H. Kim, K. Noh, C. Choi, J. Khamwannah, D. Villwock and S. Jin, *Langmuir*, 2011, 27, 10191-10196.
31. E. Balaur, J. M. Macak, H. Tsuchiya and P. Schmuki, *J. Mater. Chem.*, 2005, 15, 4488-4491.
32. S. Barthwal, Y. S. Kim and S.-H. Lim, *Journal of Colloid and Interface Science*, 2013, 400, 123-129.
33. Y. K. Lai, C. J. Lin, H. Wang, J. Y. Huang, H. F. Zhuang and L. Sun, *Electrochem. Commun.*, 2008, 10, 387-391.
34. Y. K. Lai, Y. C. Chen, Y. X. Tang, D. G. Gong, Z. Chen and C. J. Lin, *Electrochem. Commun.*, 2009, 11, 2268-2271.
35. W. Navarrini, T. Brivio, D. Capobianco, M. Diamanti, M. Pedefferri, L. Magagnin and G. Resnati, *J Coat Technol Res*, 2011, 8, 153-160.
36. S. C. Vanithakumari, R. P. George and U. Kamachi Mudali, *Applied Surface Science*, 2014, 292, 650-657.
37. S. Barthwal, Y. S. Kim and S. H. Lim, *Journal of Colloid and Interface Science*, 2013, 400, 123-129.
38. D. O. Hutchins, O. Acton, T. Weidner, N. Cernetic, J. E. Baio, D. G. Castner, H. Ma and A. K. Y. Jen, *Applied Surface Science*, 2012, 261, 908-915.
39. B. S. Smith, S. Yoriya, L. Grissom, C. A. Grimes and K. C. Popat, *Journal of Biomedical Materials Research Part A*, 2010, 95A, 350-360.
40. G. A. Crawford, N. Chawla, K. Das, S. Bose and A. Bandyopadhyay, *Acta Biomaterialia*, 2007, 3, 359-367.
41. T. Shokuhfar, G. K. Arumugam, P. A. Heiden, R. S. Yassar and C. Friedrich, *ACS Nano*, 2009, 3, 3098-3102.
42. J.-p. Zou and R.-z. Wang, *Transactions of Nonferrous Metals Society of China*, 2012, 22, 627-633.
43. M. F. Ashby, *Acta Metallurgica*, 1989, 37, 1273-1293.
44. A. Mohammadpour and K. Shankar, *J. Mater. Chem.*, 2010, 20, 8474-8477.
45. D. A. Wang, L. F. Liu, F. X. Zhang, K. Tao, E. Pippel and K. Domen, *Nano Lett.*, 2011, 11, 3649-3655.
46. A. M. Puziy, O. I. Poddubnaya, R. P. Socha, J. Gurgul and M. Wisniewski, *Carbon*, 2008, 46, 2113-2123.
47. M. J. Ariza, E. Rodriguez-Castellon, R. Rico, J. Benavente, M. Munoz and M. Oleinikova, *Journal of Colloid and Interface Science*, 2000, 226, 151-158.
48. E. S. Gawalt, G. Lu, S. L. Bernasek and J. Schwartz, *Langmuir*, 1999, 15, 8929-8933.
49. V. I. Nefedov, Y. A. Buslaev, Kuznetso.Aa and L. F. Yankina, *Zhurnal Neorganicheskoi Khimii*, 1974, 19, 1416-1417.
50. C. Viornerly, Y. Chevolut, D. Leonard, B. O. Aronsson, P. Pechy, H. J. Mathieu, P. Descouts and M. Gratzel, *Langmuir*, 2002, 18, 2582-2589.
51. K. M. Kruszewski and E. S. Gawalt, *Langmuir*, 2011, 27, 8120-8125.
52. B. M. Silverman, K. A. Wieghaus and J. Schwartz, *Langmuir*, 2005, 21, 225-228.
53. D. K. Owens and R. C. Wendt, *Journal of Applied Polymer Science*, 1969, 13, 1741-1747.
54. F. M. Fowkes, *Industrial & Engineering Chemistry*, 1964, 56, 40-52.
55. C. J. Van Oss, R. J. Good and M. K. Chaudhury, *Langmuir*, 1988, 4, 884-891.
56. T. Hata, Y. Kitazaki and T. Saito, *The Journal of Adhesion*, 1987, 21, 177-194.
57. M. D. Doganci, C. E. Cansoy, I. O. Ucar, H. Y. Erbil, E. Mielczarski and J. A. Mielczarski, *Journal of Applied Polymer Science*, 2012, 124, 2100-2109.
58. Y. Lai, C. Lin, J. Huang, H. Zhuang, L. Sun and T. Nguyen, *Langmuir*, 2008, 24, 3867-3873.
59. R. N. Wenzel, *Industrial and Engineering Chemistry*, 1936, 28, 988-994.

60. A. B. D. Cassie and S. Baxter, *Transactions of the Faraday Society*, 1944, 40, 0546-0550.
61. *The drop spreads significantly faster on substrates with bare nanotube surfaces and forms very small contact angles, hence we have reported it as the contact angle less than 5 degrees.* .
62. P.-G. De Gennes, F. Brochard-Wyart and D. Quéré, *Capillarity and wetting phenomena: drops, bubbles, pearls, waves*, Springer, 2004.
63. P. R. Waghmare, S. Das and S. K. Mitra, *Soft Matter*, 2013, 9, 7437-7447.
64. P. R. Waghmare, S. Das and S. K. Mitra, *Soft Matter*, 9, 7437-7447.
65. H. Y. Erbil and C. E. Cansoy, *Langmuir*, 2009, 25, 14135-14145.
66. O. Zenasni, A. C. Jamison and T. R. Lee, *Soft Matter*, 2013, 9, 6356-6370.
67. J. N. Israelachvili, *Intermolecular and surface forces: revised third edition*, Academic press, 2011.
68. R. E. Johnson and R. H. Dettre, in *Wettability*, ed. J. C. Berg, Marcel Dekker, New York, 1993.
69. C. Ran, G. Ding, W. Liu, Y. Deng and W. Hou, *Langmuir*, 2008, 24, 9952-9955.
70. R.-D. Sun, A. Nakajima, A. Fujishima, T. Watanabe and K. Hashimoto, *The Journal of Physical Chemistry B*, 2001, 105, 1984-1990.
71. S. Farsinezhad, A. Mohammadpour, A. N. Dalrymple, J. Geisinger, P. Kar, M. J. Brett and K. Shankar, *J. Nanosci. Nanotechnol.*, 2013, 13, 2885-2891.